A magnetic resonance study of MoS_2 fullerene-like nanoparticles

2009 J. Phys.: Condens. Matter 21 395301

(http://iopscience.iop.org/0953-8984/21/39/395301)

J. Phys.: Condens. Matter **21** (2009) 395301 (6pp) doi:10.1088/0953-8984/21/39/395301

A magnetic resonance study of MoS_2 fullerene-like nanoparticles

A M Panich[1,3], A I Shames[1], R Rosentsveig[2] and R Tenne[2]

[1] Department of Physics, Ben-Gurion University of the Negev, PO Box 653, Beer-Sheva 84105, Israel
[2] Department of Materials and Interfaces, Weizmann Institute for Science, Rehovot 76100, Israel

E-mail: pan@bgu.ac.il

Received 18 May 2009, in final form 18 August 2009
Published 1 September 2009
Online at stacks.iop.org/JPhysCM/21/395301

Abstract

We report on the first nuclear magnetic resonance (NMR) and electron paramagnetic resonance (EPR) investigation of inorganic fullerene-like MoS_2 nanoparticles. Spectra of bulk 2H-MoS_2 samples have also been measured for comparison. The similarity between the measured quadrupole coupling constants and chemical shielding anisotropy parameters for bulk and fullerene-like MoS_2 reflects the nearly identical local crystalline environments of the Mo atoms in these two materials. EPR measurements show that fullerene-like MoS_2 exhibits a larger density of dangling bonds carrying unpaired electrons, indicative of them having a more defective structure than the bulk sample. The latter observation explains the increase in the spin–lattice relaxation rate observed in the NMR measurements for this sample in comparison with the bulk 2H-MoS_2 ones.

(Some figures in this article are in colour only in the electronic version)

1. Introduction

After the discovery of carbon fullerenes and nanotubes, it was suggested that layered inorganic compounds could also form fullerene-like (IF) and tubular nanostructures (INT). Very soon after, several examples of such nanoparticles, i.e., molybdenum, tungsten and niobium dichalcogenide and boron nitride fullerene-like and nanotube species, were successfully synthesized [1–6]. The behavior of carbon nanostructures was found to be different from that of bulk graphite. While graphite is known to be a semi-metal [7–9], solid C_{60} is a semiconductor [10]. Carbon nanotubes exhibit metallic or semiconducting behavior depending on the wrapping angle (or (n, m) index) [11]. In contrast, boron nitride nanotubes are wide-gap semiconductors irrespective of their helicity [12, 13]. Boron nitride fullerenes are wide-gap semiconductors as well [14, 15].

The knowledge of the physical properties of inorganic fullerene-like MS_2 (M = Mo, W and Nb) species, for short IF-MS_2, and the respective nanotubes (INT-MS_2) is still very limited. These compounds are usually prepared from the hexagonal polytype of the transition metal dichalcogenides 2H-MS_2, whose crystal structure consists of triple S–M–S sandwich layers that are bound to one another by weak van der Waals forces and contain two layers in the unit cell. Bulk 2H-MoS_2 and 2H-WS_2 compounds are semiconductors, while 2H-NbS_2 shows metallic behavior and becomes a superconductor at very low temperatures. The detailed crystal and electronic structures of IF-MS_2 have not been determined, although the respective nanotubes have been studied quite thoroughly from both experimental and theoretical perspectives. Thus it is often implied that the hexagonal symmetry of the 2H-MS_2 lattice is locally preserved in inorganic fullerene-like structures, except for presumably the rhombic-like or triangular-like edge regions connecting three or four flat surfaces or edges between two such flat faces [16]. However, formation of a perfect fullerene-like or polyhedral structure by folding of a triple-layered MS_2 compound seems to be difficult. Furthermore, it is not known how the metal–chalcogen chemical bonds and M–S and M–M distances are affected by the curvature of the layer. Such information is necessary both from the scientific point of view and also due to the various applications of the IF, which are known to be excellent solid lubricants and are suggested for many other applications: in polymer nanocomposites, etc [17].

[3] Author to whom any correspondence should be addressed.

In this paper, we report on the first nuclear magnetic resonance (NMR) and electron paramagnetic resonance (EPR) investigation of IF-MoS_2. The spectrum of a bulk 2H-MoS_2 sample was also measured for comparison. While registration of the EPR spectra in bulk and fullerene-like MoS_2 is a routine procedure, Mo NMR measurements for solids encounter essential difficulties. Molybdenum has two magnetic isotopes: ^{95}Mo with natural abundance of 15.7% and ^{97}Mo with natural abundance 9.5%. Both isotopes have nuclear spin $I = 5/2$, and their gyromagnetic ratios differ by ∼2%. Both isotopes possess quadrupole moments and thus their spectra are sensitive to the electric field gradient that exists at a nuclear site of non-cubic symmetry. This contribution gives rise to a large linewidth of the powder spectra. Low resonance frequency, low nuclear abundance and large linewidth lead to severe difficulties in observing the Mo NMR spectra for powder samples. The next noticeable constraint on NMR data acquisition is the very long spin–lattice relaxation times of non-metallic specimens. Therefore there are only a few Mo NMR measurements available for solids, and some of them were made using ^{95}Mo enriched samples [18].

To our knowledge, the only measurement of a ^{95}Mo NMR spectrum for bulk solid 2H-MoS_2 with natural abundance of the ^{95}Mo isotope has been made by Bastow [19], who described the aforementioned difficulties in detail. Since it was initially impossible to obtain a signal from commercially available polycrystalline MoS_2, Bastow first measured the spectrum of a single crystal and only then, eventually, the spectrum of the respective powder. The line shape of the latter looked like one dominated by chemical shielding anisotropy; but, after comparing with the ^{95}Mo NMR spectra of MoS_2 and $MoSe_2$, he suggested that the line shape is caused by both chemical shielding anisotropy and second-order quadrupolar interaction. We will discuss his data along with the results of our measurements.

2. Experimental details

All experiments were performed on macroscopic powder samples of bulk 2H-MoS_2 and IF-MoS_2. The latter was prepared from the bulk by reacting MoO_3 and H_2S as described elsewhere [20–22]. A typical transmission electron microscopy (TEM) image of an IF-MoS_2 nanoparticle is shown in figure 1. It has a polyhedral onion-like structure of ∼40 nm size and usually consists of 20–30 closely stacked MoS_2 layers with the interlayer distance of 0.62 nm. The latter value is in good agreement with the interlayer spacing in bulk 2H-MoS_2.

In this study, the ^{95}Mo NMR spectra were obtained using a Tecmag Apollo 360 Pulse Solid State NMR spectrometer in the external magnetic field 8.0196 T, corresponding to the ^{95}Mo resonance frequency 22.217 MHz. The spectra were recorded using frequency-shifted and summed Fourier transform processing technique [23]. The spin–lattice relaxation time T_1 was measured by means of a saturation comb sequence. The shift of the NMR line was compared with that of anhydrous sodium molybdate, Na_2MoO_4, which has a cubic spinel structure. Therefore the Mo nucleus in Na_2MoO_4 does not experience quadrupole interaction and exhibits a sharp ^{95,97}Mo line, which makes the compound suitable as a chemical shift reference for Mo NMR spectra [19]. ^{95}Mo NMR spectra simulations were carried out using DMfit2009 software [24].

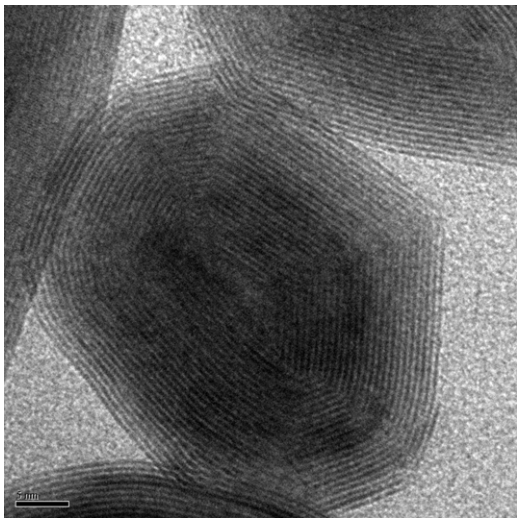

Figure 1. Characteristic TEM image of a typical IF-MoS_2 particle under study.

The effective precession rate of the nuclear magnetization around B_1 in the rotating frame for the $-1/2 \rightarrow 1/2$ quadrupolar perturbed transition is greater, and the required $\pi/2$ pulse is shorter, by a factor $(I + 1/2)$ than that for the same nucleus in the absence of a quadrupole coupling, or for an equivalent $I = 1/2$ nucleus with the same gyromagnetic ratio [25]. In our experiment, the maximum amplitude of the echo signal was achieved at ∼1/3 of the length of a $\pi/2$ pulse for equivalent ^{95}Mo nuclei in cubic Na_2MoO_4, which agrees with the above conclusion.

In the present study, we also attempted to observe an NMR signal from the ^{97}Mo isotope, whose resonance frequency in the magnetic field 8.0196 T is 22.7 MHz.

EPR spectra of powder MoS_2 samples were recorded using a Bruker EMX-220 X-band ($\nu \sim 9.4$ GHz) spectrometer equipped with an Agilent 53150A frequency counter. Processing of the EPR spectra were done using Bruker WIN-EPR and OriginLab™ software. The densities of the paramagnetic centers observed in the present experiments were estimated by comparison of doubly integrated intensities of the $g = 2.0$ signals with the intensity of the radical-like signal in a well purified nanodiamond sample with a known amount of paramagnetic defects ($N_s = 6.3 \times 10^{19}$ spins g^{-1}) [26].

All of the measurements were carried out at ambient conditions.

3. Results and discussion

3.1. ^{95}Mo NMR spectra and spin–lattice relaxation

The room temperature ^{95}Mo NMR spectra of bulk and IF samples are shown in figure 2. The 2H-MoS_2 compound has a hexagonal structure which belongs to the space group D^4_{6h}–$P6_3/mmc$ with $a = 3.162$ Å and $c = 12.295$ Å; the S–S

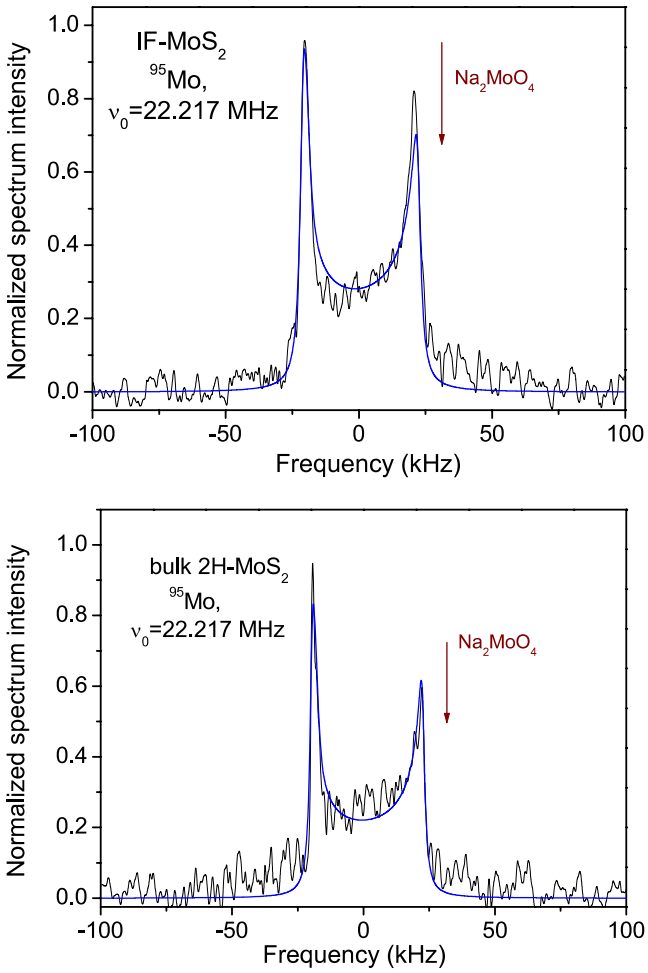

Figure 2. Experimental room temperature ^{95}Mo NMR spectra of bulk 2H-MoS_2 (bottom) and IF-MoS_2 (top) samples (black lines) and the simulated spectra (smooth blue lines). The arrow shows the position of the ^{95}Mo NMR signal for Na_2MoO_4.

distance is 3.47 Å and the Mo–S distance is 2.41 Å [27, 28]. The structure consists of S–Mo–S layers that are stacked together due to weak van der Waals forces. Each layer is composed of a hexagonal array of Mo atoms in the plane sandwiched between two sheets of sulfur atoms. Each Mo atom is surrounded by six equidistant sulfur atoms at the vertices of a trigonal prism, thus occupying a site with threefold symmetry (point symmetry group D_{3h}). Such crystal structure of 2H-MoS_2 results in an axially symmetric electric field gradient and chemical shielding tensors. Moreover, as is well known, in the hexagonal layered crystals the principal axes of the above tensors are directed perpendicular to the plane and therefore coincide.

Since the ^{95}Mo isotope is a quadrupolar nucleus and possesses spin $I = 5/2$, the ^{95}Mo NMR line shape is expected to be mainly caused by the quadrupolar interaction. If the Zeeman term is much larger than the quadrupolar one, the latter is treated as a perturbation to the Zeeman interaction. For a spin-5/2 nucleus, the quadrupolar perturbed NMR spectrum consists of five transitions. The first-order effects do not affect the central $1/2 \rightarrow -1/2$ transition that is observed at the Larmor frequency, while four satellite lines ($5/2 \rightarrow 3/2$, $3/2 \rightarrow 1/2$, $-1/2 \rightarrow -3/2$ and $-3/2 \rightarrow -5/2$ transitions) are shifted to frequencies which are determined by the product of $\nu_Q = (\frac{e^2qQ}{h})\frac{3}{2I(2I-1)}$ and an angular function related to the orientation of the applied magnetic field in the EFG principal axis frame. (Here eQ is the quadrupole moment of the nucleus and q is the electric field gradient). For a powder, the satellite lines are distributed over the frequency range of the order of $4\nu_Q$ and thus are hardly detectable. Therefore, usually only the central transition, whose shape is determined by the second-order quadrupolar effects, is observed. For the axially symmetric electric field gradient ($\eta = 0$) caused by the axial symmetry of the Mo site, the second-order shift of the central component is [29, 30]

$$\nu\left(\frac{1}{2} \leftrightarrow -\frac{1}{2}\right) = -\left(\frac{\nu_Q^2}{16\nu_0}\right)\left[I(I+1) - \frac{3}{4}\right](1-\mu^2)(9\mu^2-1). \quad (1)$$

Here $\mu = \cos\theta$, where θ is the angle between the principal axis of the electric field gradient and the applied magnetic field, and ν_0 is the Larmor frequency in the absence of electric quadrupole interaction. For a powder sample, the angular dependence of equation (1) gives rise to a line shape that possesses two maxima corresponding to $\mu = 0$ and $\mu^2 = 5/9$, and a small step discontinuity appearing at $\nu = \nu_0$, though usually being smoothed by dipolar broadening. The spacing between the two peaks is

$$\Delta = \nu_1 - \nu_2 = \frac{25\nu_Q^2}{144\nu_0}\left[I(I+1) - \frac{3}{4}\right] \quad (2)$$

with $[I(I+1) - 3/4] = 8$, $\nu_Q = \frac{3}{20}(\frac{e^2qQ}{h})$ and $\Delta = \frac{25\nu_Q^2}{18\nu_0}$ for $I = 5/2$. Our measurements reveal nearly the same splittings: $\Delta = 41.2$ and 41.6 kHz for IF and bulk samples, respectively.

At first glance, such spectra with two peaks have been observed in our experiment (figure 2), revealing the classical picture characteristic of a second-order quadrupolar perturbed $1/2 \rightarrow -1/2$ transition. However, it is well known that the quadrupolar splitting Δ is inversely proportional to the resonance frequency (equation (2)). Therefore, a smaller splitting could be expected for the ^{95}Mo NMR spectrum of bulk 2H-MoS_2, measured under an external magnetic field of 9.4 T corresponding to the resonance frequency 26.060 MHz [19]. Surprisingly, this measurement revealed almost the same spectrum splitting (around 42.7 kHz) as was obtained in our experiment [19]. The only way to reconcile the present data with those of Bastow [19] is to include an additional contribution coming from the chemical shielding anisotropy. In the case of heavy nuclei such as ^{95}Mo, this term may significantly contribute to the NMR line shape for powder samples (see, for example, the recent extensive review on NMR of the quadrupolar nuclei in powders [31]). For the axially symmetric shielding tensor, this contribution is described by the expression

$$\nu = \nu_0[1 + \alpha(3\mu^2 - 1)]. \quad (3)$$

For a powder sample, the line shape exhibits a maximum at $\theta = 90°$ ($\sigma_\perp$, $\mu = 0$), at the frequency point $\nu_1 = \nu_0(1-\alpha)$, and a shoulder at $\theta = 0°$($\sigma_\parallel$, $\mu = 1$), at the frequency point

$\nu_2 = \nu_0(1 + 2\alpha)$, where $\alpha = \sigma_\perp$ and $\sigma_\parallel$ and $\sigma_\perp$ are the parallel and perpendicular components of the chemical shielding tensor. Combined nuclear quadrupole and anisotropic chemical shift effects in a single crystal result in the following expression for the central transition frequency [30]:

$$\nu\left(\frac{1}{2} \leftrightarrow -\frac{1}{2}\right) = \nu_0\left\{1 + \left(\frac{\nu_Q^2}{16\nu_0}\right)\left[I(I+1) - \frac{3}{4}\right] \times (1-\mu^2)(9\mu^2 - 1) + \alpha(3\mu^2 - 1)\right\}. \quad (4)$$

For a polycrystalline sample, the line shape function possesses two singularities, at $\mu = 0$ and at $\mu = (\frac{5}{9} - \frac{\alpha\nu_0^2}{6b})^{1/2}$, and a step at $\mu = 1$, with $b = \frac{\nu_Q^2}{16}[I(I+1) - \frac{3}{4}]$ and a splitting between the maxima

$$\Delta = \nu_2 - \nu_1 = \frac{25b}{9\nu_0} - \frac{5}{3}\alpha\nu_0 + \frac{\alpha^2\nu_0^3}{4b} = \frac{25\nu_Q^2}{18\nu_0} - \frac{5}{3}\alpha\nu_0 + \frac{\alpha^2\nu_0^3}{2\nu_Q^2} \quad (5)$$

taking into account that $b = \frac{\nu_Q^2}{2}$ for $I = 5/2$. Spectra simulation and least square fitting using DMfit2009 software yielded two sets of the NMR parameters corresponding to negative and positive chemical shielding anisotropy, respectively, that satisfy the obtained line shape requirement. In the first set the quadrupole frequency $\nu_Q = 578 \pm 15$ kHz, quadrupole coupling constant (QCC) $\frac{e^2qQ}{h} = 3.85 \pm 0.1$ MHz, and $\Delta\sigma = (\sigma_\parallel - \sigma_\perp) = -33.53$ kHz $= -1510 \pm 80$ ppm were determined for IF-MoS_2. For bulk MoS_2 we obtained $\nu_Q = 565 \pm 25$ kHz, $\frac{e^2qQ}{h} = 3.77 \pm 0.16$ MHz, $\Delta\sigma = (\sigma_\parallel - \sigma_\perp) = -32.6$ kHz $= -1470 \pm 100$ ppm. The second set corresponds to the quadrupole frequency $\nu_Q = 1133 \pm 15$ kHz, $\frac{e^2qQ}{h} = 7.55 \pm 0.1$ MHz, and $\Delta\sigma = (\sigma_\parallel - \sigma_\perp) = 75.41$ kHz $= 3394 \pm 100$ ppm for IF-MoS_2 and $\nu_Q = 1138 \pm 20$ kHz, $\frac{e^2qQ}{h} = 7.59 \pm 0.13$ MHz, $\Delta\sigma = (\sigma_\parallel - \sigma_\perp) = 80.774$ kHz $= 3636 \pm 300$ ppm for bulk MoS_2. One can see that the values of ν_Q and $\Delta\sigma$ are nearly the same for bulk 2H-MoS_2 and fullerene-like MoS_2 nanoparticles for both sets of NMR parameters. Taking into account that the spectrum of bulk 2H-MoS_2 reported in [19] corresponds to $\Delta\sigma < 0$, the first set of parameters seems to be preferable. Simulated spectra corresponding to these parameters are shown in figure 2.

Spin–lattice relaxation measurements yielded very long relaxation times T_1 of 255 s and 122 s for bulk MoS_2 and IF-MoS_2, respectively. The reduced spin–lattice relaxation time in IF-MoS_2 in comparison with that in the bulk MoS_2 sample is mainly attributed to the larger density of paramagnetic defects and to the interaction of the nuclear spins with electron spins in these species, which gives rise to an effective spin–lattice relaxation channel [32]. This suggestion is confirmed by the EPR measurements presented below.

In our study, we also attempted to observe an NMR signal from the ^{97}Mo isotope, whose resonance frequency in the magnetic field 8.0196 T is 22.7 MHz. Since the quadrupole moment eQ of ^{97}Mo is 11.5 times larger than that of ^{95}Mo and since the relaxation time T_1 is proportional to $(eQ)^{-2}$, one can expect a much shorter T_1 for ^{97}Mo which could be of a great advantage in the present experiments. However, the linewidth of the central transition caused by second-order quadrupolar interaction varies as $(eQ)^2$ and thus should yield a linewidth of the order of 5.5 MHz. Therefore the ^{97}Mo NMR signal could not be detected here.

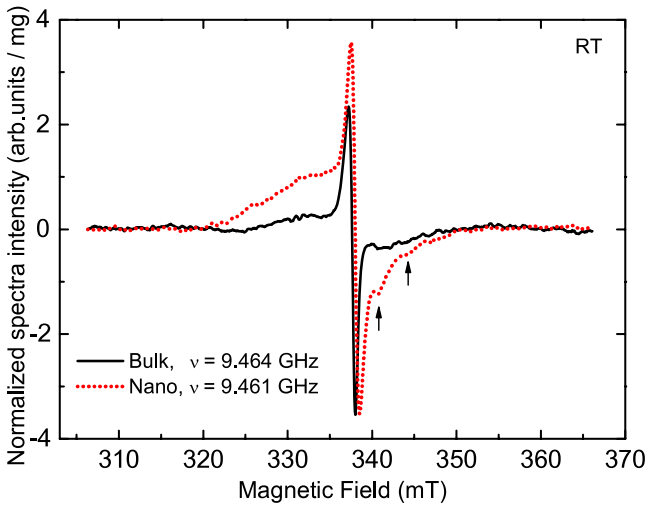

Figure 3. Room temperature EPR spectra ($g = 2.0$ region only) of bulk 2H-MoS_2 (black solid line) and IF-MoS_2 (red dotted line) samples recorded under the same experimental conditions and then normalized to unit weight. The arrows indicate additional signals in the spectrum of the IF-MoS_2 sample.

3.2. EPR spectra

The room temperature EPR spectrum of bulk 2H-MoS_2 sample shows superposition of two overlapping signals: a broad ($\Delta H_{pp} \sim 140$ mT) line with $g \sim 2.3$ (not shown) and a weak relatively narrow asymmetric line with $g_\parallel = 2.038(3)$ and $g_\perp = 2.0033(1)$ (figure 3, black solid line). The EPR spectrum of the IF-MoS_2 sample consists of a weak broad low field (resonance field $H_r \sim 50$ mT) signal and an intense narrow asymmetric signal with $g_\parallel = 2.035(3)$ and $g_\perp = 2.0026(1)$ (figure 3, red dotted line). The other two signals with $g = 1.98$ and 1.97 are distinguished on the high field wing of this signal (indicated by arrows in figure 3). The concentrations of paramagnetic species responsible for the narrow signals within the $g = 2.0$ region were estimated as 1.9×10^{16} and 1.16×10^{17} spin g^{-1} for bulk 2H-MoS_2 and the IF-MoS_2 samples, respectively.

Since Mo-inherited paramagnetic species with $g_\perp \sim 2.3$ have been observed in p-type Mo dichalcogenide crystals only at low temperatures [33], the broad signal in the EPR spectrum of the bulk 2H-MoS_2 sample originates most probably from some paramagnetic impurities (Co, Cu, Ni) and may be excluded from further consideration. The same can be said for the weak low field signal in the IF-MoS_2 sample that seems to be typical for ferromagnetic impurities. The remaining narrow signals within the $g = 2.0$ region may be considered as originating from the MoS_2 system. Signals characterized by an axially anisotropic g-factor and practically the same g-values, like in our measurements, have been observed for finely ground sulfides of MoS_2 and were ascribed to sulfur-coordinated (thio-Mo^{5+}) defects located at low symmetry edge

sites of the MoS_2 crystallites [34]. This kind of defect is the only one of its kind observed in bulk 2H-MoS_2 samples and is the predominant one in the IF-MoS_2 sample. Additional signals with $g = 1.98$ and 1.97 found in the EPR spectrum of the IF-MoS_2 sample may be attributed to other kinds of Mo^{5+}-centered local defects [35] that may involve adsorbed oxygen/OH moieties on the prismatic ($hk0$) faces of the MoS_2 platelets (2H crystallites). Following [35], any local defect in the molybdenum sulfide structure, i.e. an edge dislocation or a dangling bond, provides a paramagnetic Mo site characterized by an anisotropic g-tensor.

4. Discussion

The main contribution to the NMR spectra of IF-MoS_2 comes from the Mo atoms located on the spacious planes, while the overall number of atoms situated on the polyhedral edges is very small, and their contribution to the NMR signal is imperceptible. Thus the closeness of the quadrupole coupling constants and chemical shielding anisotropy parameters for bulk and fullerene-like MoS_2 reflects the nearly identical local crystal structures of the S–Mo–S molecular sheets of these two materials. Such a finding is expected for large 'onions' (IF-MoS_2 nanoparticles).

We note that the quadrupole coupling and chemical shielding are particularly sensitive to variations of the chemical bonding and electron charge distribution in the neighborhood of the nucleus. The charges close to the nucleus have the most important effect. A closed shell with a spherically symmetric electronic charge contributes nothing to the quadrupole coupling and shielding anisotropy; thus the contribution of the ionic bond vanishes. The essential QCC and shielding values in MoS_2 likely reflect a considerable covalency of the Mo–S bond. An analogous conclusion about predominantly covalent bonding has been reached by Lucovsky *et al* [36] who studied the infrared reflectance spectra of MoS_2. The authors reported that MoS_2 displays weak reststrahlen with effective charges of the order of $0.5e$. On the basis of the Pauling electronegativities [37] $x(\mathrm{Mo}) = 2.16$ and $x(\mathrm{S}) = 2.58$ for molybdenum and sulfur, respectively, one can estimate that a single Mo–S bond has a 96% covalent character. Since the effective charges of molybdenum and sulfur in MoS_2 are close to each other, one could expect a behavior of IF-MoS_2 similar to that of carbon nanotubes and fullerenes. However, we noticed above that this is not the case. This finding results from the difference in band structure of semi-metallic graphite and the semiconducting molybdenum sulfide. Like multiwall boron nitride nanotubes [38], MoS_2 fullerenes exhibit similar values of the QCC and ν_Q to the bulk compound. This finding reflects the very similar chemical bonding, local symmetry, and charge distribution over the Mo–S bond and would result in similar electronic properties dominated by the band structure of the hexagonal-like sheets. It seems that the Mo–S chemical bonds are strong enough to hold the Mo–S and Mo–Mo distances so that they are little affected by the weak curvature of the IF layers. One can expect only monolayer-like (single-wall) fullerenes with very small diameter and large curvature to show different electronic properties with respect to those of bulk compounds, e.g., a decrease of the band gap caused by the curvature of the sheets and the appearance of some $sp^2 \rightarrow sp^3$ re-hybridization [16].

Our recent study [39] indicated that polyhedral carbon onions have defect-free sp^2 faces and all their defects condense at their polyhedral edges. Unusual magnetic resonance features of these onions were attributed to charge carriers delocalized over the faces; the density of free carriers considerably exceeds that of spins localized in defects on the multi-shell polyhedra edges. Polyhedral IF-MoS_2 particles are made of large flat faces consisting of hexagons; these faces are connected by edge regions and vertices with presumably rhombic-like structure. By analogy with polyhedral carbon onions, one can suggest the existence of nearly defect-free MoS_2 flat faces, while a limited number of defects condense at the edges and vertices (corners) of the polyhedral fullerene particles. Our measurements show that MoS_2 fullerenes have more defective structure than the bulk sample. These defects presumably appear upon folding of the triple molybdenum sulfide sheets, when most of the side atoms at the connecting edges are stitched together, while some of them are left unbound and form various lattice defects with dangling bonds carrying unpaired electrons. Such lattice misfits evidently arise from the difficulty in forming a perfect polyhedral structure by the folding of triple MoS_2 layers, in which Mo can be bound only to S, and vice versa.

We note that Mottner *et al* [40], who measured quadrupole interactions in single-crystalline and powder 2H-MoS_2 by means of time differential perturbed angular correlation (TDPAC) spectroscopy, determined characteristic parameters $\frac{e^2qQ}{h} = 18.74$ MHz and $\eta = 0$, i.e. axial symmetry, for the excited state of ^{99}Mo with $I = 5/2$. Unfortunately, the nuclear quadrupole moment eQ of ^{99}Mo is not known. Roy and Choudhury [41] estimated it as 0.173 b for the first excited state of ^{99}Mo. Taking into account that $eQ(^{95}\mathrm{Mo}) = -0.022$ b, one can find the ratio of quadrupole coupling constants of ^{99}Mo and ^{95}Mo isotopes as 7.86, which is of the same order of magnitude as the values found from our data.

5. Summary

In summary, we report the first NMR and EPR investigation of inorganic fullerene-like MoS_2 nanoparticles. The similarity between the NMR spectral parameters of bulk 2H-MoS_2 and IF-MoS_2 reflects the nearly identical local crystal structures of the polyhedral faces of these two kinds of materials and helps to explain why the fullerene-like MoS_2 retains the electronic properties of the bulk compound. Our data show that MoS_2 fullerenes have more defective structure than the bulk sample and exhibit larger amounts of dangling bonds carrying unpaired electrons. The latter causes the increase in the spin–lattice relaxation rate in this sample in comparison with bulk 2H-MoS_2 observed in our NMR measurements.

Acknowledgments

The kind help of D Massiot with using his DMfit software [24] is greatly appreciated. RT holds the Drake Family Chair in Nanotechnology and is the director of the Helen and Martin

Kimmel Center for Nanoscale Science. His work is supported by the ERC grant INTIF 226639 and the Israel Science Foundation.

References

[1] Tenne R, Margulis L, Genut M and Hodes G 1992 *Nature* **360** 444
[2] Rapoport L, Bilik Y, Feldman Y, Homyonfer M, Cohen S R and Tenne R 1997 *Nature* **387** 791
[3] Feldman Y, Frey G L, Homyonfer M, Lyakhovitskaya V, Margulis L, Cohen H, Hodes G, Hutchison J L and Tenne R 1996 *J. Am. Chem. Soc.* **118** 5362
[4] Tenne R 2006 *Nat. Nanotechnol.* **1** 103
[5] Chopra N G, Luyken R J, Cherrey K, Crespi V H, Cohen M L, Louie S G and Zettl A 1995 *Science* **269** 966
[6] Golberg D, Bando Y, Stéphan O and Kurashima K 1998 *Appl. Phys. Lett.* **73** 2441
[7] Slonczewski J C and Weiss P R 1958 *Phys. Rev.* **109** 272
[8] McClure J W 1957 *Phys. Rev.* **108** 612
[9] Spain I L 1977 *Mater. Sci. Eng.* **31** 183
[10] Saito S and Oshiyama A 1991 *Phys. Rev. Lett.* **66** 2637
[11] Hamada N, Sawada S and Oshiyama A 1992 *Phys. Rev. Lett.* **68** 1579
[12] Rubio A, Corkill J L and Cohen M 1994 *Phys. Rev.* B **49** 5081
[13] Blase X, Rubio A, Louie S G and Cohen M L 1994 *Europhys. Lett.* **28** 355
[14] Hirano T, Oku T and Suganuma K 2000 *Diamond Relat. Mater.* **9** 625
[15] Oku T, Nishiwaki A and Narita I 2004 *Sci. Technol. Adv. Mater.* **5** 635
[16] Enyashin A N, Gemming S, Bar-Sadan M, Popovitz-Biro R, Hong S Y, Prior Y, Tenne R and Seifert G 2007 *Angew. Chem. Int. Edn* **46** 623
[17] Naffakh M, Martin Z, Fanegas N, Marco C, Gomez M A and Jimenez I 2007 *J. Polym. Sci.* B **45** 2309
[18] Mastikhin V M, Lapina O B and Maksimovskaya R I 1988 *Chem. Phys. Lett.* **148** 413
[19] Bastow T J 1998 *Solid State Nucl. Magn. Reson.* **12** 191
[20] Feldman Y, Wasserman E, Srolovitz D J and Tenne R 1995 *Science* **267** 222
[21] Srolovitz D J, Safran S A, Homyonfer M and Tenne R 1995 *Phys. Rev. Lett.* **74** 1778
[22] Feldman Y, Frey G L, Homyonfer M, Lyakhovitskaya V, Margulis L, Cohen H, Hodes G, Hutchison J L and Tenne R 1996 *J. Am. Chem. Soc.* **118** 5362
[23] Clark W G, Hanson M E and Lefloch F 1995 *Rev. Sci. Instrum.* **66** 2453
[24] Massiot D, Fayon F, Capron M, King I, Calve S L, Alonso B, Durand J O, Bujoli B, Gan Z and Hoatson G 2002 *Magn. Reson. Chem.* **40** 70
[25] Fukushima E and Roeder S B W 1981 *Experimental Pulse NMR: a Nuts and Bolts Approach* (Reading, MA: Addison-Wesley) p 109
[26] Osipov V Yu, Shames A I, Enoki T, Takai K, Baidakova M V and Vul' A Ya 2007 *Diamond Related Mater.* **16** 2035
[27] Dickinson R G and Pauling L 1923 *J. Am. Chem. Soc.* **45** 1465
[28] Hassel O 1925 *Z. Kristallogr.* **61** 92
[29] Cohen M H and Reif F 1957 *Solid State Phys.* **5** 321
[30] Jones W H, Graham T P and Barnes R G 1963 *Phys. Rev.* **132** 1898
[31] Lapina O B, Khabibulin D F, Shubin A A and Terskikh V V 2008 *Prog. Nucl. Magn. Reson. Spectrosc.* **53** 28
[32] Abragam A 1961 *The Principles of Nuclear Magnetism* (Oxford: Clarendon)
[33] Fonville R M M, Geerstma W and Haas C 1978 *Phys. Status Solidi* b **85** 621
[34] Silbernagel B G 1983 *J. Magn. Magn. Mater.* **31–34** 885
[35] Deroide B, Bensimon Y, Belougne P and Zanchetta J V 1991 *J. Phys. Chem. Solids* **52** 853
[36] Lucovsky G, White R M, Benda J A and Revelli J F 1973 *Phys. Rev.* B **7** 3859
[37] Pauling L 1960 *The Nature of the Chemical Bond* (Ithaca, NY: Cornell University Press)
[38] Panich A M, Shames A I, Froumin N, Tang C C and Bando Y 2005 *Phys. Rev.* B **72** 085307
[39] Shames A I, Katz E A, Panich A M, Mogilyansky D, Mogilko E, Grinblat J, Belousov V P, Belousova I M and Ponomarev A N 2009 *Diamond Relat. Mater.* **18** 505
[40] Mottner P, Butz T, Lerf A, Ledezma G and Knoezinger H 1995 *J. Phys. Chem.* **99** 8260
[41] Roy B B and Choudhury D C 1972 *Phys. Rev.* C **12** 323